Shape Changes in the $N = 28$ Island of Inversion: Collective Structures Built on Configuration-Coexisting States in ^{43}S

B. Longfellow,[1,2,3] D. Weisshaar,[1] A. Gade,[1,2] B. A. Brown,[1,2] D. Bazin,[1,2] K. W. Brown,[1,4] B. Elman,[1,2] J. Pereira,[1] D. Rhodes,[1,2] and M. Spieker[1,*]

[1]National Superconducting Cyclotron Laboratory, Michigan State University, East Lansing, Michigan 48824, USA
[2]Department of Physics and Astronomy, Michigan State University, East Lansing, Michigan 48824, USA
[3]Lawrence Livermore National Laboratory, Livermore, California 94550, USA
[4]Department of Chemistry, Michigan State University, East Lansing, Michigan 48824, USA

(Received 12 July 2020; revised 6 October 2020; accepted 30 October 2020; published 2 December 2020)

The neutron-rich nuclei in the $N = 28$ island of inversion have attracted considerable experimental and theoretical attention, providing great insight into the evolution of shell structure and nuclear shape in exotic nuclei. In this work, for the first time, quadrupole collectivity is assessed simultaneously on top of the $3/2^-$ ground state and the $7/2^-$ shape-coexisting isomer of ^{43}S, putting the unique interpretation of shape and configuration coexistence at $N = 27$ and 28 in the sulfur isotopic chain to the test. From an analysis of the electromagnetic transition strengths and quadrupole moments predicted within the shell model, it is shown that the onset of shape coexistence and the emergence of a simple collective structure appear suddenly in ^{43}S with no indication of such patterns in the $N = 27$ isotone ^{45}Ar.

DOI: 10.1103/PhysRevLett.125.232501

Understanding how the structure of nuclei is modified far from stability has become a major quest in modern nuclear science. While, in analogy to shells in atomic physics, the nuclear shell model [1,2] was successful in explaining the magic numbers observed for the stable and near-stable nuclei available for study at the time, subsequent research on nuclei with extreme proton-to-neutron ratios has revealed surprising nuclear-structure changes [3,4]. For example, the conventional magic number $N = 28$ breaks down in the region of neutron-rich nuclei centered around ^{44}S and ^{42}Si [5,6], known as the $N = 28$ island of inversion [7].

One particularly fascinating interplay emerges between shell evolution and the shape of nuclei in this region. The concept of nuclear shape is inherent to self-bound nuclear matter confined into a finite volume. Famously, a spherical equilibrium shape is energetically favored near magic numbers. In the case of the breakdown of the $N = 28$ magic number, however, quadrupole correlations lead to near-degenerate configurations built on the $\nu f_{7/2}$ and $\nu p_{3/2}$ neutron single-particle orbitals and the resulting deformation [8,9], which reflects the underlying SU(3) symmetry of the nucleus, has been likened to a nuclear Jahn-Teller effect [9–11]. This leads to one of the most unusual cases of shape and configuration coexistence on the nuclear chart: an isomeric 4_1^+ state in ^{44}S [12,13] that may have its decay hindered by a high K quantum number [12,14], a phenomenon typically found only in heavy nuclei with more than 100 nucleons [15,16]. This unusual configuration can be found at low excitation energy in ^{44}S in addition to shape-coexisting 0^+ states [17]. The surprising experimental discovery of multiple coexisting shapes or configurations spurred theoretical interpretations within a variety of nuclear models [8,14,18] and the importance of the odd-A neighbor ^{43}S in confirming the pictures put forth by theory has been indicated [8,14,19].

The discovery of a 320-keV isomeric state provided early evidence for shape coexistence in ^{43}S [20]. Through a g-factor measurement, the 415-ns half-life isomer was confirmed to have $7/2^-$ spin-parity [21], while the $3/2^-$ ground state appears dominated by intruder configurations, placing ^{43}S inside the $N = 28$ island of inversion. The measured spectroscopic quadrupole moment of the $7/2^-$ isomer exceeded expectations for a single-particle state, in agreement with SDPF-U shell-model calculations [22], suggesting collectivity or deformation [23]. Within the collective model, and using the K quantum numbers referenced above, the decay of the isomeric $7/2^-$ state ($K = 7/2$) is hindered due to the large K difference with the levels below (all $K = 1/2$).

In this work, collective structures in the key nucleus ^{43}S were characterized in the first simultaneous Coulomb excitation measurements made from ground and isomeric states for a fast beam. The extracted electromagnetic transition strengths are compared to predictions for these coexisting structures within shell-model approaches. Complementing the previous analyses of shell-model calculations that used angular-momentum projection approximations [14] or Kumar-Cline quadrupole invariants [8], we provide a phenomenological picture via $E2$ maps that track collective structures emerging on top of the coexisting states. It is shown that, within the SDPF-MU interaction [9], the

shape coexistence and simple collective structure emerge abruptly in ^{43}S and appear not to be present at all in ^{45}Ar.

The measurement was performed using a ^{48}Ca primary beam accelerated to 140 MeV/u with the Coupled Cyclotron Facility at the National Superconducting Cyclotron Laboratory [24]. The cocktail secondary beam consisting mainly of ^{43}S was produced by fragmentation of the primary beam on a 1034 mg/cm^2 ^{9}B production target in the A1900 fragment separator [25]. A 450 mg/cm^2 achromatic Al wedge degrader was used for secondary beam purification.

To induce Coulomb excitation, the ^{43}S secondary beam was impinged on a 492 mg/cm^2 ^{209}Bi target at the reaction-target position of the S800 spectrograph [26]. Plastic scintillators and the S800 focal-plane detectors [27] were used to identify the scattered ^{43}S event by event and reconstruct their trajectories and scattering angles. From the scattering angle, the impact parameter is inferred. At intermediate beam energies (76 MeV/u at midtarget for ^{43}S), the analysis must be restricted to a minimum impact parameter, which is chosen to exceed the sum of the radii of the projectile and target nuclei by several femtometers, to exclude nuclear contribution to the excitation [28–32].

Cross sections for populating excited states via Coulomb excitation were determined by surrounding the ^{209}Bi target with CAESAR, a high-granularity, high-efficiency array of 192 CsI(Na) scintillators [33], to detect their in-flight γ-ray deexcitations. Using the relativistic model of Coulomb excitation [34], the electric quadrupole transition strength $B(E2)$ to the populated level was deduced from the Coulomb excitation cross section. The in-beam response and energy-dependent detection efficiency of CAESAR after Doppler reconstruction were modeled using GEANT4 simulations benchmarked against laboratory-frame spectra from standard γ-ray calibration sources. Following Ref. [35], the simulated efficiency curve was scaled to match the measured efficiencies introducing a 5% systematic uncertainty.

The secondary beam production via fragmentation leaves some ^{43}S nuclei in the isomeric $7/2^-$ state. Two methods were used to determine the fraction remaining in the isomer after transportation to the ^{209}Bi reaction target. First, the ^{43}S beam was stopped at the center of CAESAR with a 5.1-mm-thick Al stopper. From the efficiency-corrected number of 320-keV γ rays from the decay of the isomer, including the loss due to absorption in the Al stopper predicted with GEANT4, divided by the number of incoming ^{43}S projectiles, the proportion of ^{43}S nuclei in the isomeric state at the center of CAESAR was established as 14(3)%. Second, the CsI(Na) hodoscope at the back of the S800 focal plane [36] in the IsoTagger configuration [37] was utilized to determine the isomeric content. In this setup, no reaction target or stopper was installed at the center of CAESAR. The hodoscope efficiency was estimated using a GEANT4 simulation of IsoTagger including the Al stopping plate before the CsI(Na) detectors and the surrounding vacuum chamber [37]. To determine the isomeric content at the reaction-target position, the half-life of the isomer must be considered. Using an average velocity of 0.396c, a 415-ns half-life, and a 15-m flight path between the reaction-target location and the IsoTagger Al stopper in the S800 focal plane, 81% of the ^{43}S nuclei remain in the isomeric state after the flight. Accounting for this yields an 18(4)% isomeric content at the reaction target. The average of the isomeric content measurements is 16(5)% where the difference in the two results was adopted as the systematic uncertainty.

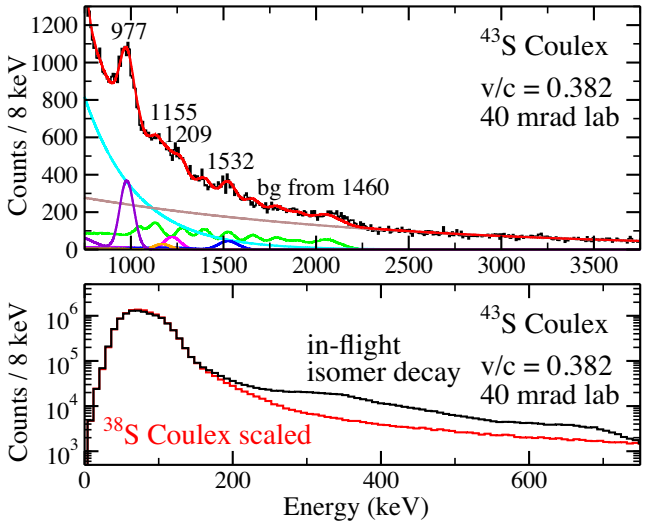

FIG. 1. Top: Doppler-corrected energy spectrum for ^{43}S gated on laboratory-frame scattering angles smaller than 40 mrad. The red curve is the total fit function. The individual GEANT4 simulations of the observed in-beam and background γ decays along with a double exponential background are shown in other colors. Bottom: Low-energy portion of the ^{43}S Doppler-corrected energy spectrum. The wide feature present for ^{43}S that is absent for ^{38}S (see Ref. [41]) is from the continuous decay of the 320-keV isomer along the beam line. The smooth low-energy background is due to bremsstrahlung and other beam-correlated background.

The higher (top) and lower (bottom) energy regions of the ^{43}S γ-ray spectrum from CAESAR after Doppler reconstruction are shown in Fig. 1 using a laboratory-frame maximum scattering angle cut of 40 mrad. No addback was applied to this spectrum to avoid additional systematic uncertainty on the energy-dependent efficiency of CAESAR. The highest-statistics peak is at 979(6) keV and has been reported previously at 971(6) [38], 977(9) [39], and 977(4) keV [40]. In Ref. [39], this transition was inferred to feed a level at 184(2) keV from lifetime measurements. However, it was noted that the observed intensities of the 184- and 977-keV γ rays were equal within uncertainties [39], as was the case in Ref. [38]. In the recent one-neutron knockout work, the intensity of the 977-keV transition was larger than the 185(1)-keV

transition intensity, establishing the 977-keV γ decay as a ground-state transition and the 185-keV γ decay as originating from the 1162-keV state [40]. As seen in the bottom panel of Fig. 1, the 185-keV transition is not observed here, supporting the ordering in Ref. [40]. However, the beam-correlated background in this low-energy region is high, challenging peak observation. Since the γ decay of the 320-keV isomer can occur anywhere along the beam line, Doppler reconstruction assuming the decay occurs at the middle of the reaction target results in the wide feature shown in the bottom panel of Fig. 1 rather than a 320-keV peak.

The top panel of Fig. 1 shows weaker peaks at 1168(27), 1219(22), and 1525(10) keV. The energies of these transitions were measured at 1154(7), 1203(7), and 1529 (9) keV in Ref. [38], at 1159(9), 1213(10), and 1543 (13) keV in Ref. [39], and at 1155(4), 1209(4), and 1532 (5) keV in Ref. [40]. The 1155-keV γ ray has been placed in the ^{43}S level scheme as a ground-state transition [38–40], as has the 1209-keV γ ray [40]. In this work, no γ-γ coincidence relationships were observed with CAESAR, supporting these previous placements. The prompt 1532-keV transition was measured in coincidence with the isomeric 320-keV decay in the hodoscope [40]. Here, additional evidence consistent with the 1532-keV transition feeding the 320-keV isomer is seen in Fig. 2, which shows the CAESAR spectrum for multiplicity-one events after nearest-neighbor addback in coincidence with the 320-keV peak measured in the hodoscope with background subtraction applied.

The nominal laboratory-frame safe scattering angle from the touching spheres plus 2 fm approximation is about 47 mrad. However, the angular emittance of the beam and angular straggling in the thick target lead to a reduction in counts at larger scattering angles, necessitating a more restrictive choice for the maximum scattering angle [35,42]. The angle-integrated cross section for the ^{43}S 977-keV

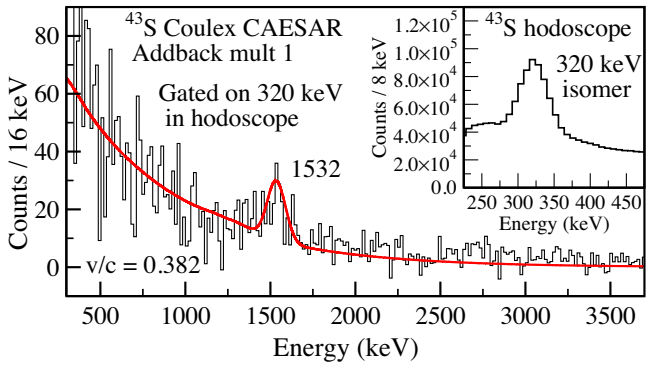

FIG. 2. Background-subtracted, Doppler-corrected energy spectrum for ^{43}S measured with CAESAR in coincidence with 320-keV γ rays detected in the hodoscope at the S800 focal plane from the decay of the isomer. The inset shows the laboratory-frame hodoscope spectrum for coincidences.

transition as a function of maximum scattering angle is provided in Ref. [41]. Using the more restrictive choice of 40 mrad, the $B(E2)$ strength from the $3/2^-$ ground state to the 977-keV level is 91(18) e^2fm^4. With the same maximum scattering angle, the $B(E2)$ strengths to the 1155- and 1209-keV states are 9(7) and 23(11) e^2fm^4, respectively. Similarly, the $B(E2)$ strength from the $7/2^-$ isomeric state at 320 keV to the 1852-keV level that decays via a 1532-keV γ-ray transition is 101(42) e^2fm^4. All $B(E2)$ strengths were calculated considering the population of the respective initial states given the ^{43}S beam isomeric content. Furthermore, SDPF-MU multipole mixing ratios were used to determine the angular distributions for mixed decays input into the GEANT4 simulations. For the 1532-keV transition, the resulting detection efficiencies using the SDPF-MU mixing ratio, the SDPF-U mixing ratio, and isotropic γ decay all agree within 1% due to CAESAR's near 4π coverage. The SDPF-MU mixing ratios were utilized to determine all quoted $B(E2)$ strengths.

In a previous intermediate-energy Coulomb excitation experiment, the $B(E2)$ strength to a level around 940 keV in ^{43}S was measured as 175(69) e^2fm^4 [43], which is almost a factor of 2 larger than the value of 91(18) e^2fm^4 to the level measured here at 979(6) keV and in Ref. [40] at 977(4) keV. It was noted by Ibbotson *et al.* that the 940-keV peak may consist of multiple γ rays within the 8% energy resolution of their detector array [43]. In this work and in the other in-beam γ-ray spectroscopy experiments [38–40], no multiplets were observed in this energy range. However, since identification of the outgoing particles in Ref. [43] relied on a phoswhich detector sensitive to Z but with an insufficient flight path for a time-of-flight measurement providing exit-channel mass resolution, γ rays following one-neutron removal into ^{42}S must have been a contaminant. The 940-keV peak energy could then be explained as the centroid of 977- and 903-keV transitions with each contributing half the counts. In fact, this is supported by the present work, where the number of 903-keV counts measured in coincidence with the ^{42}S one-neutron removal products identified with the S800 spectrograph is about 90% of the number of 977-keV counts from ^{43}S Coulomb excitation.

The lifetime of the $7/2^-_2 \rightarrow 3/2^-_1$ transition calculated from the measured $B(E2; 3/2^-_1 \rightarrow 7/2^-_2)$ strength of 91(18) e^2fm^4 is 20(4) ps. The SDPF-MU prediction is 13 ps. The lifetimes of the 977-keV and 184-keV transitions were measured by Mijatović *et al.* using the recoil-distance method [39]. The best-fit results were obtained assuming the 977-keV transition feeds the 184-keV transition which is shown to be incorrect in Ref. [40].

$B(E2)$ strengths for low-lying states in ^{43}S predicted from the SDPF-MU interaction using the full *sd* (proton) and full *pf* (neutron) model space with proton and neutron effective charges of 1.35 and 0.35, respectively [9], are shown in Fig. 3 along with the present results. For the work presented here, the *p* orbitals have been shifted up

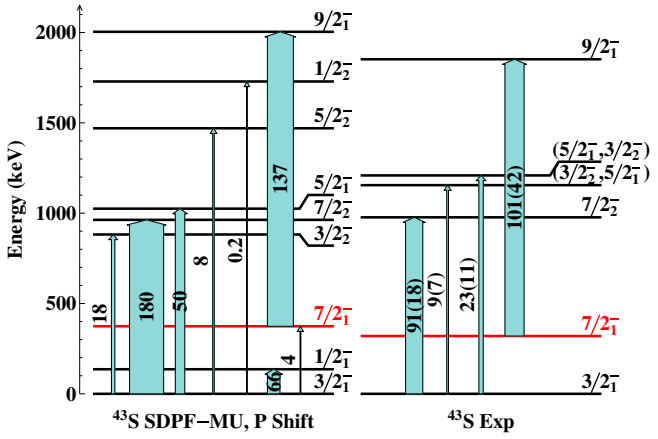

FIG. 3. SDPF-MU predictions for $B(E2)$ strengths in $e^2\mathrm{fm}^4$ for low-lying levels in ^{43}S compared with experimental results. The p orbitals have been shifted up by 300 keV to improve agreement with the energy of the $7/2^-_1$ isomer (red). This modification has a negligible effect on the calculated transition strengths. Arrow widths are proportional to $B(E2)$.

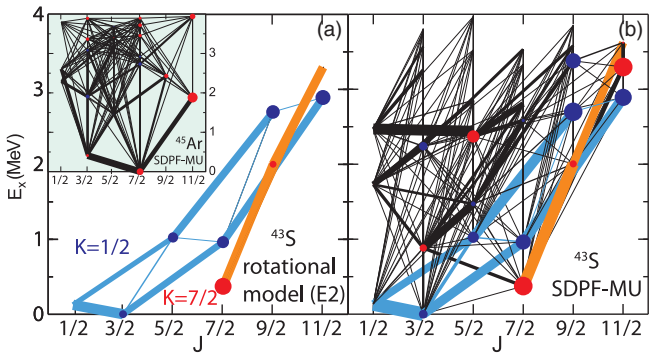

FIG. 4. $E2$ map for ^{43}S (a) in the collective model for $K = 1/2$ and $7/2$ using $Q_i = 50\ e\mathrm{fm}^2$ and (b) for our SDPF-MU calculations (p orbitals moved up by 300 keV). The size of the dots signifies the magnitude of the Q_s moment and the color its sign (blue, negative; red, positive). The $B(E2\downarrow)$ strength connecting the states is indicated by the line thickness. The emergence of the simple collective structure in the complex shell-model calculation is clearly visible. The inset shows the $E2$ map for ^{45}Ar, exhibiting no such distinct collective structures or shape coexistence.

by 300 keV to reproduce the energy of the $7/2^-_1$ state (SDPF-MU). Based on the intensity of the experimentally observed 977-keV transition, the 977-keV level is assigned as the $7/2^-_2$ state, establishing it as a member of the rotational band built on top of the intruder $3/2^-$ ground state. However, the experimental $B(E2)$ strength of $91(18)\ e^2\mathrm{fm}^4$ is 2 times smaller than the predicted value of $180\ e^2\mathrm{fm}^4$. The 1155- and 1209-keV states are most similar to the shell-model $3/2^-_2$ and $5/2^-_1$ levels. SDPF-MU predicts that the $3/2^-_2$ and $5/2^-_1$ states decay predominantly to the ground state (100%) with only 29% and 16% relative branching ratios to all other levels, respectively. The second largest branching ratios are to the low-lying $1/2^-$ state, which has been tentatively reported at 228 keV [40] but was not observed here, possibly due to the high low-energy beam-correlated background seen in Fig. 1. Since these other decay branches would result in 927- and 981-keV γ rays, a portion of the $B(E2)$ strength to the 1155- and 1209-keV states may be misattributed to the 977-keV state.

Finally, the 1852-keV state is assigned as the $9/2^-_1$ level on top of the $7/2^-_1$ isomer. The $B(E2)$ strength predicted from SDPF-MU is 137 $e^2\mathrm{fm}^4$, while the measured value is $101(42)\ e^2\mathrm{fm}^4$. The predicted energy of 2004 keV is also in good agreement with the measured value. Note that the predicted $B(E2)$ strength from the isomer to the $11/2^-_2$ level is 63 $e^2\mathrm{fm}^4$. The $11/2^-_2$ state, at 3297 keV in the calculation, has relative branching ratios of 100% to the $7/2^-_1$ isomer and 49% to the $9/2^-_1$ state and therefore could provide unobserved feeding to the $9/2^-_1$ level. As discussed in Ref. [23], the normal-order configuration provides the largest contribution to the wave function of the isomer but intruder configurations also play a role. For example, the experimental spectroscopic quadrupole moment $|Q_s|$ of $23(3)\ e\mathrm{fm}^2$ is larger than expected for a single-hole state and well reproduced by shell-model calculations [23]. Here, the measured $B(E2; 7/2^-_1 \rightarrow 9/2^-_1)$ strength is smaller than but in agreement within uncertainty with the shell-model prediction, supporting the general picture of shape coexistence painted by SDPF-MU. In Ref. [40], the 1856(7)-keV transition was suggested as a possible ground-state decay from the 1852-keV level based on its energy. Because of the large spin difference between the $3/2^-$ ground state and the $9/2^-$ level at 1852 keV established here, the 1856-keV transition is strongly suggested to originate from a different level.

It is interesting to examine the nature of the collectivity built on the ground state and the $7/2^-$ isomer. This was done for SDPF-U shell-model calculations with quadrupole invariants by Chevrier and Gaudefroy [8]. We complement that work here by tracking bandlike structures built on top of these states within the SDPF-MU shell model. Figure 4 shows the calculated states for a given J^- value and indicates the $B(E2\downarrow)$ strength and sign (indicating shape) and magnitude for the Q moment for ^{43}S within the collective model [Fig. 4(a)], the SDPF-MU shell model [Fig. 4(b)], and its $N = 27$ isotone ^{45}Ar (inset). Using intrinsic quadrupole moments of $Q_i = 50\ e\mathrm{fm}^2$ in the collective model gives $Q_s(7/2^-_1) = +23\ e\mathrm{fm}^2$ and $B(E2)$ values of $127\ e^2\mathrm{fm}^4$ for $3/2^-_1 \rightarrow 7/2^-_2$ and $105\ e^2\mathrm{fm}^4$ for $7/2^-_1 \rightarrow 9/2^-_1$, all in agreement with experiment. For ^{43}S, the $K = 1/2$ and $7/2$ bands within this simple collective model emerge in the SDPF-MU shell-model calculation, in agreement with Ref. [14]. In fact, the corresponding intraband transitions are the strongest links in the $E2$ map. In contrast, comparable structures and low-lying states with large and opposite-sign Q_s are absent in ^{45}Ar, indicating that the descent into the $N = 28$ island of inversion is steep with a sudden onset of shape coexistence

and simple collective structures at $Z = 16$. Quantitatively, the experimental results agree with both SDPF-U and SDPF-MU calculations and the collective model in that the intraband $B(E2\uparrow)$ values built atop the ground and $7/2^-$ isomer are large and approximately equal [44].

In summary, collective levels in $N = 27$ ^{43}S were probed using intermediate-energy Coulomb excitation. By utilizing an incoming ^{43}S beam with isomeric content, states on top of both the intruder $3/2^-$ ground state and the $7/2^-$ isomeric state were Coulomb excited simultaneously for the first time. The strongest $E2$ transitions built on each of the two states are approximately equal, in agreement with SDPF-U and SDPF-MU shell-model calculations. This supports the robust picture put forth by both models of shape coexistence caused by a nuclear Jahn-Teller effect in light of the near degeneracy of the $\nu p_{3/2}$ and $\nu f_{7/2}$ single-particle states due to shell evolution and the breakdown of the $N = 28$ magic number and the sudden emergence of a simple collective structure that is absent in the neighboring isotone ^{45}Ar.

This work was supported by the National Science Foundation (NSF) under Grants No. PHY-1102511 and No. PHY-1565546, by the DOE National Nuclear Security Administration through the Nuclear Science and Security Consortium, under Award No. DE-NA0003180, and by the Department of Energy, Office of Nuclear Physics, under Grant No. DE-SC0020451. Work at LLNL was performed under Contract No. DE-AC52-07NA27344. B. A. B. acknowledges support from NSF Grant No. PHY-1811855. Discussions with K. Wimmer are gratefully acknowledged.

*Present address: Department of Physics, Florida State University, Tallahassee, Florida 32306, USA.

[1] M. G. Mayer, Phys. Rev. **75**, 1969 (1949).
[2] O. Haxel, J. H. D. Jensen, and H. E. Suess, Phys. Rev. **75**, 1766 (1949).
[3] O. Sorlin and M.-G. Porquet, Prog. Part. Nucl. Phys. **61**, 602 (2008).
[4] T. Otsuka, A. Gade, O. Sorlin, T. Suzuki, and Y. Utsuno, Rev. Mod. Phys. **92**, 015002 (2020).
[5] T. Glasmacher, B. A. Brown, M. J. Chromik, P. D. Cottle, M. Fauerbach, R. W. Ibbotson, K. W. Kemper, D. J. Morrissey, H. Scheit, D. W. Sklenicka, and M. Steiner, Phys. Lett. B **395**, 163 (1997).
[6] B. Bastin *et al.*, Phys. Rev. Lett. **99**, 022503 (2007).
[7] E. Caurier, F. Nowacki, and A. Poves, Phys. Rev. C **90**, 014302 (2014).
[8] R. Chevrier and L. Gaudefroy, Phys. Rev. C **89**, 051301(R) (2014).
[9] Y. Utsuno, T. Otsuka, B. A. Brown, M. Honma, T. Mizusaki, and N. Shimizu, Phys. Rev. C **86**, 051301(R) (2012).
[10] P.-G. Reinhard and E. Otten, Nucl. Phys. **A420**, 173 (1984).
[11] W. Nazarewicz, Nucl. Phys. **A574**, 27 (1994).
[12] J. J. Parker *et al.*, Phys. Rev. Lett. **118**, 052501 (2017).
[13] D. Santiago-Gonzalez, I. Wiedenhöver, V. Abramkina, M. L. Avila, T. Baugher, D. Bazin, B. A. Brown, P. D. Cottle, A. Gade, T. Glasmacher, K. W. Kemper, S. McDaniel, A. Rojas, A. Ratkiewicz, R. Meharchand, E. C. Simpson, J. A. Tostevin, A. Volya, and D. Weisshaar, Phys. Rev. C **83**, 061305(R) (2011).
[14] Y. Utsuno, N. Shimizu, T. Otsuka, T. Yoshida, and Y. Tsunoda, Phys. Rev. Lett. **114**, 032501 (2015).
[15] G. D. Dracoulis, Phys. Scr. **T152**, 014015 (2013).
[16] G. D. Dracoulis, P. M. Walker, and F. G. Kondev, Rep. Prog. Phys. **79**, 076301 (2016).
[17] C. Force *et al.*, Phys. Rev. Lett. **105**, 102501 (2010).
[18] J. L. Egido, M. Borrajo, and T. R. Rodríguez, Phys. Rev. Lett. **116**, 052502 (2016).
[19] M. Kimura, Y. Taniguchi, Y. Kanada-En'yo, H. Horiuchi, and K. Ikeda, Phys. Rev. C **87**, 011301(R) (2013).
[20] F. Sarazin *et al.*, Phys. Rev. Lett. **84**, 5062 (2000).
[21] L. Gaudefroy *et al.*, Phys. Rev. Lett. **102**, 092501 (2009).
[22] F. Nowacki and A. Poves, Phys. Rev. C **79**, 014310 (2009).
[23] R. Chevrier *et al.*, Phys. Rev. Lett. **108**, 162501 (2012).
[24] A. Gade and B. M. Sherrill, Phys. Scr. **91**, 053003 (2016).
[25] D. Morrissey, B. Sherrill, M. Steiner, A. Stolz, and I. Wiedenhoever, Nucl. Instrum. Methods Phys. Res., Sect. B **204**, 90 (2003).
[26] D. Bazin, J. Caggiano, B. Sherrill, J. Yurkon, and A. Zeller, Nucl. Instrum. Methods Phys. Res., Sect. B **204**, 629 (2003).
[27] J. Yurkon, D. Bazin, W. Benenson, D. Morrissey, B. Sherrill, D. Swan, and R. Swanson, Nucl. Instrum. Methods Phys. Res., Sect. A **422**, 291 (1999).
[28] T. Glasmacher, Annu. Rev. Nucl. Part. Sci. **48**, 1 (1998).
[29] A. Gade, D. Bazin, C. M. Campbell, J. A. Church, D. C. Dinca, J. Enders, T. Glasmacher, Z. Hu, K. W. Kemper, W. F. Mueller, H. Olliver, B. C. Perry, L. A. Riley, B. T. Roeder, B. M. Sherrill, and J. R. Terry, Phys. Rev. C **68**, 014302 (2003).
[30] A. Gade and T. Glasmacher, Prog. Part. Nucl. Phys. **60**, 161 (2008).
[31] J. M. Cook, T. Glasmacher, and A. Gade, Phys. Rev. C **73**, 024315 (2006).
[32] F. Delaunay and F. M. Nunes, J. Phys. G **34**, 2207 (2007).
[33] D. Weisshaar, A. Gade, T. Glasmacher, G. F. Grinyer, D. Bazin, P. Adrich, T. Baugher, J. M. Cook, C. A. Diget, S. McDaniel, A. Ratkiewicz, K. P. Siwek, and K. A. Walsh, Nucl. Instrum. Methods Phys. Res., Sect. A **624**, 615 (2010).
[34] A. Winther and K. Alder, Nucl. Phys. **A319**, 518 (1979).
[35] B. Elman, A. Gade, D. Weisshaar, D. Barofsky, D. Bazin, P. C. Bender, M. Bowry, M. Hjorth-Jensen, K. W. Kemper, S. Lipschutz, E. Lunderberg, N. Sachmpazidi, N. Terpstra, W. B. Walters, A. Westerberg, S. J. Williams, and K. Wimmer, Phys. Rev. C **96**, 044332 (2017).
[36] K. Meierbachtol, D. Bazin, and D. J. Morrissey, Nucl. Instrum. Methods Phys. Res., Sect. A **652**, 668 (2011).
[37] K. Wimmer, D. Barofsky, D. Bazin, L. M. Fraile, J. Lloyd, J. R. Tompkins, and S. J. Williams, Nucl. Instrum. Methods Phys. Res., Sect. A **769**, 65 (2015).
[38] L. A. Riley, P. Adrich, T. R. Baugher, D. Bazin, B. A. Brown, J. M. Cook, P. D. Cottle, C. A. Diget, A. Gade, D. A. Garland, T. Glasmacher, K. E. Hosier, K. W. Kemper,

A. Ratkiewicz, K. P. Siwek, J. A. Tostevin, and D. Weisshaar, Phys. Rev. C **80**, 037305 (2009).
[39] T. Mijatović, N. Kobayashi, H. Iwasaki, D. Bazin, J. Belarge, P. C. Bender, B. A. Brown, A. Dewald, R. Elder, B. Elman, A. Gade, M. Grinder, T. Haylett, S. Heil, C. Loelius, B. Longfellow, E. Lunderberg, M. Mathy, K. Whitmore, and D. Weisshaar, Phys. Rev. Lett. **121**, 012501 (2018).
[40] S. Momiyama, K. Wimmer, D. Bazin, J. Belarge, P. Bender, B. Elman, A. Gade, K. W. Kemper, N. Kitamura, B. Longfellow, E. Lunderberg, M. Niikura, S. Ota, P. Schrock, J. A. Tostevin, and D. Weisshaar, Phys. Rev. C **102**, 034325 (2020).
[41] B. Longfellow, Ph.D. Thesis, Michigan State University, 2020.
[42] V. M. Bader, A. Gade, D. Weisshaar, B. A. Brown, T. Baugher, D. Bazin, J. S. Berryman, A. Ekström, M. Hjorth-Jensen, S. R. Stroberg, W. B. Walters, K. Wimmer, and R. Winkler, Phys. Rev. C **88**, 051301(R) (2013).
[43] R. W. Ibbotson, T. Glasmacher, P. F. Mantica, and H. Scheit, Phys. Rev. C **59**, 642 (1999).
[44] We note that the shell-model calculation can be brought into better agreement with experiment by lowering the neutron effective charge from 0.35 to 0.25. The possible reasons for the smaller effective charge will be discussed in an upcoming paper on $B(E2)$ strengths in the even sulfur isotopes.